PHYSICAL REVIEW B **87**, 180501(R) (2013)

Superconductivity in Cu_xIrTe_2 driven by interlayer hybridization

M. Kamitani,[1,*] M. S. Bahramy,[2] R. Arita,[1] S. Seki,[1] T. Arima,[3] Y. Tokura,[1,2] and S. Ishiwata[1]

[1]*Department of Applied Physics and Quantum-Phase Electronics Center (QPEC), University of Tokyo, Hongo, Tokyo 113-8656, Japan*

[2]*RIKEN Center for Emergent Matter Science (CEMS), Wako, Saitama 351-0198, Japan*

[3]*Department of Advanced Materials Science, University of Tokyo, Kashiwa 277-8561, Japan*

(Received 25 December 2012; published 2 May 2013)

The change in the electronic structure of layered Cu_xIrTe_2 has been characterized by transport and spectroscopic measurements, combined with first-principles calculations. The Cu intercalation suppresses the monoclinic distortion, giving rise to the stabilization of the trigonal phase with superconductivity. Thermopower and Hall resistivity measurements suggest the multiband nature with hole and electron carriers for this system, which is masked by the predominance of the hole carriers enhanced by the interlayer hybridization in the trigonal phase. Rather than the instability of the Ir d band, a subtle balance between the interlayer and intralayer Te-Te hybridizations is proposed as a main factor dominating the structural transition and the superconductivity.

DOI: 10.1103/PhysRevB.87.180501 PACS number(s): 74.70.Xa, 74.20.Pq, 74.25.F−

The proximity of a superconducting phase to the other quantum ordered phase provides a fertile ground for emergent electronic features. Transition-metal dichalcogenides, MX_2, with layered structure have provided renewed interest for the apparently strong interplay between superconducting and charge density wave (CDW) instability, which is implicated by the trace of the CDW transition temperature falling on top of the domelike T_c curve as a function of control parameter, e.g., carrier density or composition.[1–5] $IrTe_2$ with Pt or Pd doping is one such new example but has an additional feature in terms of spin-orbit interaction (SOI).[6,7] Materials with strong SOI have received growing attention for novel helical spin textures in reciprocal space or real space found in topological insulators[8] and chiral magnets,[9,10] respectively. In addition, superconductivity realized in topological insulators with a spin nondegenerate Fermi surface is expected to have an unconventional gap symmetry.

$IrTe_2$ shows a structural phase transition from a high-temperature trigonal to a low-temperature monoclinic phase at around 250 K.[11] A recent study using a transmission electron microscope has revealed the presence of the superlattice modulation with a propagation vector of $\boldsymbol{q} = (1/5,0,-1/5)$, assigned to a CDW modulation.[7] Considering the partially filled t_{2g} orbitals indicated from their local density approximation calculation, orbitally driven Peierls instability was proposed as an origin of the structural transition.[7] The importance of the orbital degree of freedom for the transition was also pointed out from the x-ray photoemission spectroscopy of the Ir $4f$ core level.[12] On the other hand, Fang *et al.* have postulated that the reduction of the kinetic energy of Te p bands rather than the Peierls instability plays a key role in the structural transition.[13] Despite the extensive studies on $IrTe_2$ with chemical substitutions, the origin of the structural transition and its relation to superconductivity are yet to be clarified.

In this Rapid Communication, we report on transport measurements, x-ray absorption spectroscopy (XAS), and theoretical calculations for Cu-intercalated $IrTe_2$ prepared by low-temperature reaction. The monoclinic phase in $IrTe_2$ is dramatically suppressed and the superconductivity appears by the Cu intercalation. The Cu ion not only works as an n-type dopant but also affects the orbital hybridizations in $IrTe_2$. The density functional theory calculations combined with experimental results have revealed the importance of the interlayer orbital hybridization for the structural phase transition.

Polycrystalline samples of Cu_xIrTe_2 were synthesized by two steps, including intercalation reaction in evacuated quartz tubes. First, $IrTe_2$ polycrystals were prepared from the stoichiometric mixture of Ir and Te powders. The mixture was heated at 900 °C for 20 h, after which the sample pressed into pellets was annealed in the same condition. Second, $IrTe_2$ and Cu powders mixed in appropriate stoichiometry were pressed into pellets and heated at 300 °C for 200 h with one intermediate grinding. Note that an impurity phase of CuTe appears, when the Cu intercalation process was performed at higher temperatures than 400 °C or a stoichiometric mixture of Cu, Ir, and Te was heated at 900 °C. Therefore, the low-temperature intercalation reaction is necessary for the preparation of the pure Cu_xIrTe_2 phase. The samples were characterized by powder x-ray diffractions with Cu $K\alpha$ radiation. The Ir L-edge XAS measurements were performed at 4C beamline in Photon Factory, Japan. The electrical resistivity and Hall resistivity were measured through a five-probe technique with Physical Property Measurement System (PPMS; Quantum Design). The thermopower was measured through a steady-state technique with PPMS, and the contribution from the voltage lead was subtracted. Magnetization measurements were carried out with a superconducting quantum interference device magnetometer. The electronic-structure calculations were carried out using the full-potential augmented plane-wave plus local orbital methods, as implemented in the WIEN2K code.[14] The exchange-correlation part of the potential was treated using the Perdew-Burke-Ernzerhof exchange-correlation functional.[15] The maximum modulus of reciprocal vectors K_{max} and muffin-tin radii of atoms R_{MT} were chosen such that $R_{MT}K_{max} = 7$. The lattice parameters were taken from experiment[11] and the corresponding Brillouin zone of trigonal phase (monoclinic phase) was sampled by a $20 \times 20 \times 20$ ($8 \times 15 \times 10$) k mesh.

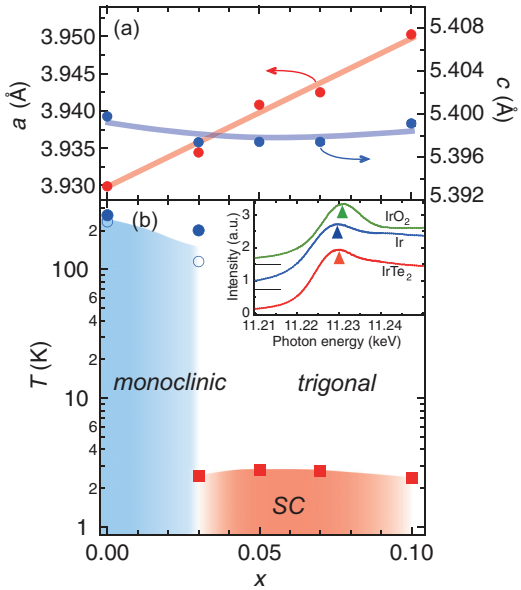

FIG. 1. (Color online) (a) In-plane and out-of-plane lattice constants and (b) electronic phase diagram of Cu_xIrTe_2 as a function of x. Solid lines in (a) are a guide to the eyes. Filled circles and open circles in (b) indicate the critical temperatures for structural phase transition on heating and cooling, respectively. Filled squares correspond to the superconducting transition temperature. The inset shows Ir L_3-edge x-ray absorption spectra for IrO_2, Ir, and $IrTe_2$ taken at room temperature. The spectra for Ir and IrO_2 are shifted upward for clarity. The absorption peak positions are indicated by the filled triangles.

$IrTe_2$ crystallizes in the 1T-TaS_2 (or CdI_2) type trigonal structure (P-3m1) at room temperature.[16] As in the case for $Cu_{0.5}IrTe_2$, Cu^+ ions are expected to be incorporated into the octahedral site in between the Te-Te double layers.[17] This is because the Cu ions were reacted at 300 °C, which is much lower compared to the previous work,[17,18] and no impurity phase of Ir compounds was detected after the Cu intercalation. With increasing the Cu content x, the a-axis length increases monotonically, reflecting the reduction of the valence of Ir ions [see Fig. 1(a)]. The change in the a-axis length, $\Delta a/a$, with increasing x from 0 to 0.1 in Pd_xIrTe_2 is less than 0.2%,[7] whereas that of Cu_xIrTe_2 is 0.5%, indicating that the valence of Ir ions in Cu_xIrTe_2 changes more effectively upon the chemical doping. On the other hand, the c-axis length remains almost constant in the range of $0 \leqslant x \leqslant 0.1$ in agreement with the previous work,[11,17] but in contrast to the case for Cu_xTiSe_2 showing elongation of the c-axis length by the accommodation of Cu ions.[3] The suppression of the elongation along the c axis with increasing x in Cu_xIrTe_2 can be ascribed to the strong hybridization between the Cu s orbitals and the Te p orbitals. The inset of Fig. 1(b) shows Ir L_3-edge XAS for $IrTe_2$ together with the references of IrO_2 and Ir, measured at room temperature. The absorption-edge energy of $IrTe_2$ is closer to that of Ir rather than IrO_2, suggesting that the effective valence of the Ir ions in the trigonal phase is not +4 but should be much lower. This result is consistent with the band structure calculation, as discussed later. The change in XAS spectra by the Cu intercalation is too small to be discerned (data not shown).

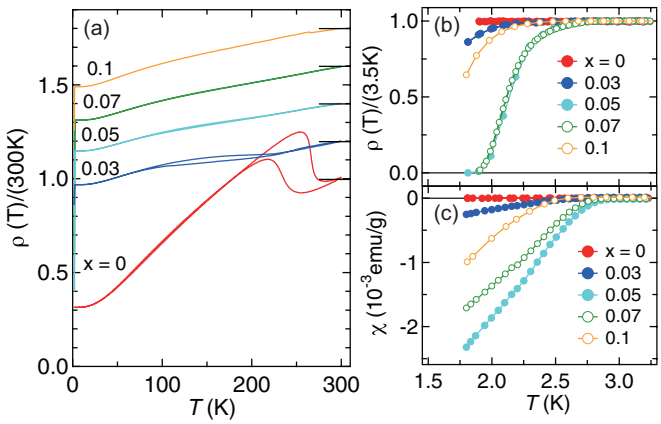

FIG. 2. (Color online) (a) Temperature dependence of normalized resistivity ρ (T)/ρ (300 K) of Cu_xIrTe_2 with x ($0 \leqslant x \leqslant 0.1$). ρ (T)/ρ (300 K) for Cu-doped samples are shifted upwards by 0.2 for clarity. Temperature dependence of (b) ρ (T)/ρ (3.5 K) without external magnetic fields and (c) magnetic susceptibility under a magnetic field of 10 Oe.

Figure 2(a) shows the temperature dependence of resistivity for Cu_xIrTe_2. All the samples show a metallic behavior. The anomaly with large thermal hysteresis around 200–250 K in $IrTe_2$ can be associated with the structural phase transition from the trigonal to monoclinic form.[11] The hump-shaped anomaly broadens and shifts to lower temperature by the Cu intercalation of $x = 0.03$, and almost disappears for $x = 0.05$, where the trigonal phase is stabilized down to the lowest temperature and the superconductivity with T_c (onset) = 2.8 K emerges, as shown in Figs. 2(b) and 2(c). Zero resistivity and clear shielding signals are observed for the samples with $x = 0.05$ and 0.07, while for the samples with $x = 0.03$ and 0.1 faint indications of superconductivity are found at lower temperatures. The Cu intercalation for $IrTe_2$ acts as electron doping in the similar manner for Cu_xTiSe_2.[5] As observed for the Pt or Pd doped $IrTe_2$,[6,7] the similar superconducting dome can be confirmed for Cu_xIrTe_2 in the vicinity of the phase boundary between the trigonal and monoclinic phases.

Next, we show Seebeck coefficient S and Hall coefficient R_H of Cu_xIrTe_2, both of which are less affected by the grain boundaries and thus suitable for characterizing the electronic properties of the polycrystalline samples [see Figs. 3(a) and 3(c)]. The sign of S is positive in all compositions and whole temperature range. This is semiquantitatively reproduced by the density functional theory calculation, as the calculated S values for the monoclinic and trigonal phases with $x = 0$ are positive over the whole temperature [see Fig. 3(b)].

However, while R_H is positive for the Cu-intercalated compounds, it becomes negative below 100 K in the monoclinic phase of $IrTe_2$, reflecting the difference in the Fermi surfaces of both phases and the multiband nature of the monoclinic phase. S of $IrTe_2$ shows a kink at 200—250 K, which reflects the reconstruction of the Fermi surface across the structural transition, and gradually increases with decreasing temperature down to 50 K. Such a behavior in S is almost smeared out for $Cu_{0.03}IrTe_2$. Here, we introduce the following

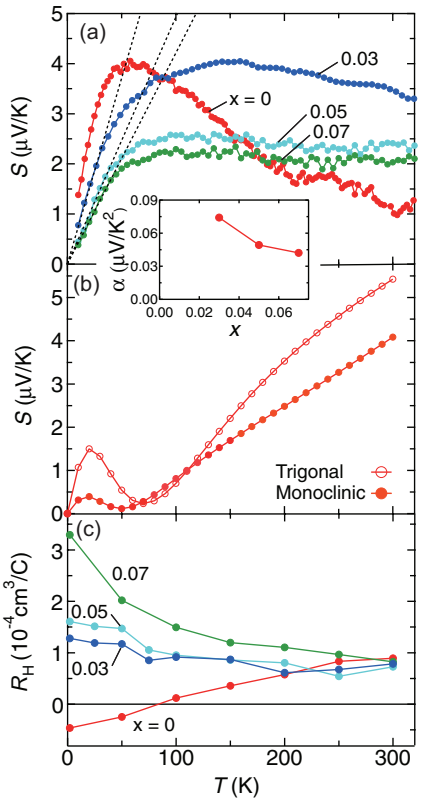

FIG. 3. (Color online) Temperature dependence of (a) Seebeck coefficient measured on cooling for Cu_xIrTe_2, (b) calculated Seebeck coefficient, and (c) Hall coefficient. The broken lines in panel (a) are the fit to the data at low temperatures based on the equation $S = \alpha T$. The inset shows the variation of α as a function of the Cu content x.

expressions of S and R_H for a two-band system with electron and hole carriers:[19]

$$S = \frac{n_h\mu_h S_h + n_e\mu_e S_e}{n_h\mu_h + n_e\mu_e}, \tag{1}$$

$$R_H = \frac{(n_h\mu_h^2 - n_e\mu_e^2)}{e(n_h\mu_h + n_e\mu_e)^2}. \tag{2}$$

Here, n_h, μ_h, and S_h represent the carrier concentration, mobility, and Seebeck coefficient for the hole band, respectively, and n_e, μ_e, and S_e represent those for the electron band. From these equations, it is found that the sign reversal between R_H and S as well as the temperature-dependent sign reversal of R_H in the monoclinic phase is a hallmark of the multiband with electron and hole carriers.

On the other hand, the multiband nature is masked in the trigonal phase by the strong interlayer hybridization giving rise to the predominance of hole conduction through the Te $5p$ band [as seen in Fig. 4(a) and Ref. 13]. Therefore, we have performed a semiquantitative analysis for the trigonal phase with a single-carrier model. Taking a look at Fig. 3(c) with assuming this model, the increase of the positive value of R_H at 2 K on going from $x = 0.03$ to $x = 0.07$ can be interpreted as the monotonic decrease of hole concentration n upon increasing x. Below 30 K, S for the Cu-intercalated compounds obeys linear temperature dependence in accordance with the diffusive thermopower in a metallic system.[20] With assuming

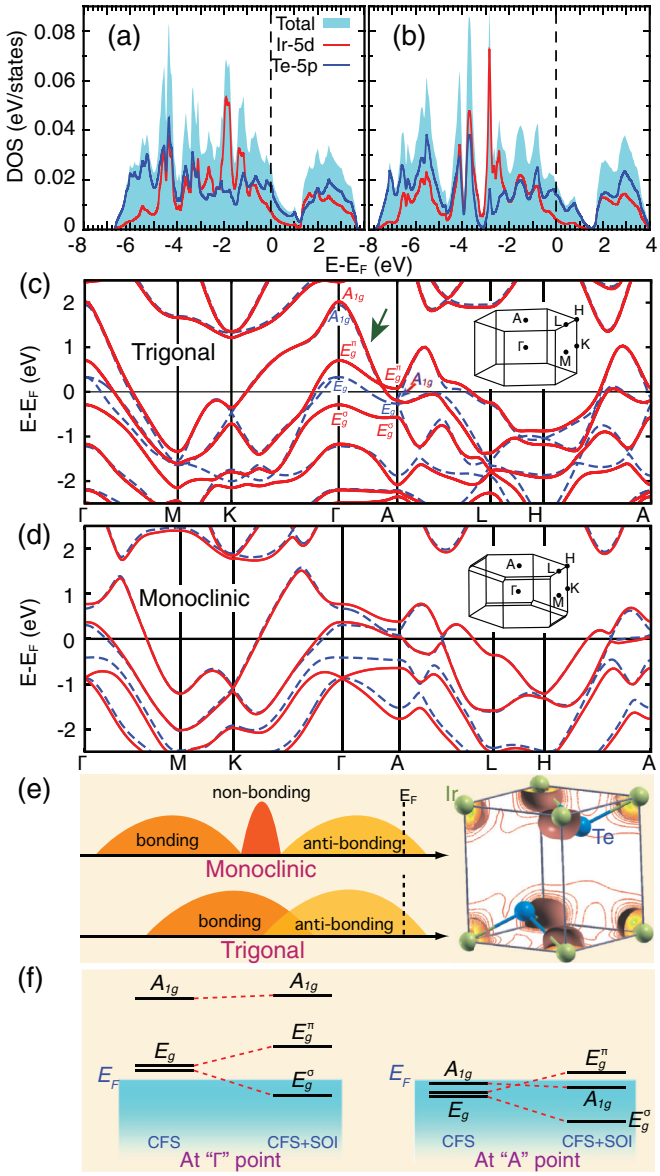

FIG. 4. (Color online) Calculated density of states of $IrTe_2$ in (a) the trigonal phase and (b) the monoclinic phase. The respective band structures near the Fermi level are shown in (c) and (d). The solid (red) and dashed (red) lines correspond to the band dispersions obtained with and without inclusion of SOI, respectively. (e) Relative positioning of bonding and antibonding states in each phase. The monoclinic phase has additionally nonbonding states [corresponding to the states spanning energies from −3 eV to −4.6 eV in (b)] which are mainly localized on Ir atoms. The electron density distribution of these states is shown in the inset. For the trigonal phase, the interplay between the CFS and SOI at the Γ and A points is schematically shown in (f).

the quasi-two-dimensional (2D) parabolic band,[21] S can be described by the following equation:

$$S = -\frac{\pi k_B^2}{2e\hbar^2 d}\frac{m^*}{n}T, \tag{3}$$

where $2\pi\hbar$, k_B, d, n, and m^* represent the Planck constant, the Boltzmann constant, distance between the adjacent conduction layers, carrier concentration, and effective mass, respectively.

With the use of Eq. (3), m^* for $Cu_{0.05}IrTe_2$ is calculated to be $4.3m_0$ (m_0 being the bare electron mass) by adopting the estimated carrier concentration at 2 K ($n = 3.9 \times 10^{22}$ cm^{-3}) and the fitting parameter α in the formula $S = \alpha T$. This value is much larger than that estimated from the band calculation ($m^* = 0.6$–$2.4m_0$). The discrepancy in magnitude between the experimental and the calculated m^* as well as S is likely to arise from the finite electron correlation in addition to the simplicity of the model. Nevertheless, the decrease in α with increasing x from 0.03 to 0.07 [see the inset of Fig. 3(b)] can be ascribed to the decrease in m^* rather than the increase in n, which is supported by the band calculation and the Hall coefficient data. This interpretation for S qualitatively explains the change in the electronic specific-heat coefficient in the trigonal phase of $Ir_{1-x}Pt_xTe_2$.[6]

Let us discuss the origin of structural phase transition in $IrTe_2$ and its relation to the superconductivity, based on the result of density functional theory calculations. As shown in Figs. 4(a) and 4(b), the calculated densities of states (DOS) of trigonal and monoclinic phases reveal that the Ir d states are widely spread below the Fermi level (E_F) with only a minor portion of them left unoccupied. Thus, the nominal valence of Ir is neither +3 nor +4, but should be much lower. In fact, our calculated Wannier charges suggest that Ir (Te) loses (gains) only $1.1e$ ($0.5e$) in the trigonal phase, which appears to be in good agreement with our XAS measurements. Due to this rather weak Ir-Te bonding, what possibly derives the phase transition in this material is the Te-Te interaction. In the high-temperature trigonal phase, this interaction is much stronger between the Te atoms of neighboring layers than those within the same $IrTe_2$ layer. Because of this, the interlayer Te-Te distance d_{Te} becomes smaller than d_{Te} within the same layer [3.498 Å compared with 3.557 and 3.928 Å (Ref. 16)]. Consequently, the electronic bands around E_F become highly dispersive in all directions, especially along the c axis [corresponding to the Γ-A direction as indicated by the arrow in Fig. 4(c)]. Due to this strong interaction, the bonding and antibonding states of Te can strongly overlap with each other through Ir d states. The emergence of superconductivity can be associated with the stabilization of the quasi-three-dimensional holelike Fermi surface in the trigonal phase.

Lowering the temperature into the monoclinic phase, the bonding states move to the lower energies, allowing the system to reduce its total energy. Such an energy reduction results in the formation of a nonbonding region between the bonding and antibonding states mainly localized on Ir atoms, as shown in Fig. 4(e). As the overlap between the bonding and antibonding states has been reduced, the interlayer interaction is substantially suppressed. On the other hand, as the bonding states have moved to lower energies, the interaction of Te atoms within the same layer is enhanced; the interlayer (intralayer) d_{Te} increases (decreases) to 4.036 Å [3.083 Å and 3.812 Å (Ref. 16)]. This also results in a considerable reduction in the Ir-Te bond length and hence enhances the d-p hybridization. The overall effect of these changes is that the Ir-Ir bonds become relatively elongated along one of the in-plane axes, therefore resulting in a phase transition to the monoclinic phase. In the monoclinic phase, the interlayer interaction and hence the band dispersion along the c axis (Γ-A direction) are suppressed, therefore the 2D character of the Fermi-surface (FS) topology becomes enhanced [see Fig. 4(d)]. Such a change in the topology of FS along the k_z direction due to the phase transition appears to be consistent with what has been observed in angle-resolved photoemission spectroscopy measurements.[22]

At this point, it is worth briefly explaining the role of crystal field splitting (CFS) and SOI on the electronic band dispersions of $IrTe_2$. As shown in Figs. 4(c) and 4(d), the electronic states around E_F are more dramatically modified by SOI in the trigonal phase than in the monoclinic phase. Without SOI, in the former phase, due to the trigonal CFS, the predominantly p-type states are split into the twofold degenerate E_g and singlefold A_{1g} bands. Such a splitting substantially decreases in going from the Γ point to A point due to the strong interlayer hybridization between Te atoms, thereby making both bands occupied in the vicinity of the A point. Turning on SOI, however, the E_g bands are split off by nearly 1 eV into E_g^σ and E_g^π branches such that the former (latter) one is pushed below (above) E_F. Given the strong (weak) CFS at the Γ (A) point, the overall effect of SOI appears as a change in the ordering of E_g^π and A_{1g} bands along the Γ-A direction, as schematically depicted in Fig. 4(f). The reported topological complexity of Fermi surface in the trigonal phase[7] is thus expected to be due to strong interplay between the trigonal CFS and SOI.

In summary, we have experimentally and theoretically studied the superconducting Cu_xIrTe_2 synthesized by low-temperature intercalation reaction. Thermopower and Hall resistivity reveal the multiband nature with electron and hole carriers in the monoclinic phase and the predominance of hole carriers in the trigonal phase stabilized by the Cu doping. Contrary to the previous reports,[6,7,12] the band structure calculations combined with XAS measurements suggest that the valence of Ir ions is much lower than +4, and the dramatic change in the interlayer and intralayer hybridizations plays an important role in the structural phase transition, rather than the instability of Ir t_{2g} orbitals. These results imply that the suppression of the monoclinic phase and the emergence of superconductivity are not only caused by the chemical potential shift in the rigid band but by the enhancement of interlayer orbital hybridization. The highly dispersive bands along the c axis, which come from the strong interlayer hybridization, are expected to play an important role in producing the superconductivity in this multiband system.

The authors thank H. Sakai for enlightening discussions. This study was in part supported by the Grant-in-Aid for Scientific Research (Grant No. 23685014) from the MEXT, and by Funding Program for World-Leading Innovative R&D on Science and Technology (FIRST Program), Japan.

*kamitani@ce.t.u-tokyo.ac.jp

[1] J. A. Wilson and A. D. Yoffe, Adv. Phys. **18**, 193 (1969).

[2] A. H. Castro Neto, Phys. Rev. Lett. **86**, 4382 (2001).

[3] E. Morosan, H. W. Zandbergen, B. S. Dennis, J. W. G. Bos, Y. Onose, T. Klimczuk, A. P. Ramirez, N. P. Ong, and R. J. Cava, Nat. Phys. **2**, 544 (2006).

[4]E. Morosan, K. E. Wagner, Liang L. Zhao, Y. Hor, A. J. Williams, J. Tao, Y. Zhu, and R. J. Cava, Phys. Rev. B **81**, 094524 (2010).
[5]D. Qian, D. Hsieh, L. Wray, E. Morosan, N. L. Wang, Y. Xia, R. J. Cava, and M. Z. Hasan, Phys. Rev. Lett **98**, 117007 (2007).
[6]S. Pyon, K. Kudo, and M. Nohara, J. Phys. Soc. Jpn. **81**, 053701 (2012).
[7]J. J. Yang, Y. J. Choi, Y. S. Oh, A. Hogan, Y. Horibe, K. Kim, B. I. Min, and S-W. Cheong, Phys. Rev. Lett. **108**, 116402 (2012).
[8]M. Z. Hasan and C. L. Kane, Rev. Mod. Phys. **82**, 3045 (2010).
[9]S. Mühlbauer, B. Binz, F. Jonietz, C. Pfleiderer, A. Rosch, A. Neubauer, R. Georgii, and P. Böni, Science **323**, 915 (2009).
[10]X. Z. Yu, Y. Onose, N. Kanazawa, J. H. Park, J. H. Han, Y. Matsui, N. Nagaosa, and Y. Tokura, Nature (London) **465**, 901 (2010).
[11]N. Matsumoto, K. Taniguchi, R. Endoh, H. Takano, and S. Nagata, J. Low Temp. Phys. **117**, 1129 (1999).
[12]D. Ootsuki, Y. Wakisaka, S. Pyon, K. Kudo, M. Nohara, M. Arita, H. Anzai, H. Namatame, M. Taniguchi, N. L. Saini, and T. Mizokawa, Phys. Rev. B **86**, 014519 (2012).
[13]A. F. Fang, G. Xu, T. Dong, P. Zheng, and N. L. Wang, Sci. Rep. **3**, 1153 (2013).
[14]P. Blaha, K. Schwarz, G. Madsen, D. Kvasnicka, and J. Luitz, WIEN2K package, version 10.1, http://www.wien2k.at.
[15]J. P. Perdew, K. Burke, and M. Ernzerhof, Phys. Rev. Lett. **77**, 3865 (1996).
[16]S. Jobic, P. Deniard, R. Brec, J. Rouxel, A. Jouanneaux, and A. N. Fitch, Z. Anorg. Allg. Chem. **598**, 199 (1991).
[17]S. Nagata, N. Kijima, S. Ikeda, N. Matsumoto, R. Endoh, S. Chikazawa, I. Shimono, and H. Nishihara, J. Phy. Chem. Solids **60**, 163 (1999).
[18]Y. S. Hor, A. J. Williams, J. G. Checkelsky, P. Roushan, J. Seo, Q. Xu, H. W. Zandbergen, A. Yazdani, N. P. Ong, and R. J. Cava, Phys. Rev. Lett. **104**, 057001 (2010).
[19]H. Yoshino, K. Murata, N. Shirakawa, Y. Nishihara, Y. Maeno, and T. Fujita, J. Phys. Soc. Jpn. **65**, 1548 (1996).
[20]P. E. Nielsen and P. L. Taylor, Phys. Rev. B **10**, 4061 (1974).
[21]J. B. Mandal, A. N. Das, and B. Ghosh, J. Phys.: Condens. Matter **8**, 3047 (1996).
[22]D. Ootsuki, S. Pyon, K. Kudo, M. Nohara, M. Horio, T. Yoshida, A. Fujimori, M. Arita, H. Anzai, H. Namatame, M. Taniguchi, N. L. Saini, and T. Mizokawa, arXiv:1207.2613.